
























Nuclear Winds Drive Large-Scale Cold Gas Outflows in Quasars during the Reionization Epoch

YONGDA ZHU ¹ MARCIA J. RIEKE ¹ LUIS C. HO ^{2,3} YANG SUN ¹ GEORGE H. RIEKE ¹ FENG YUAN ⁴
TOM J. L. C. BAKX ⁵ GEORGE D. BECKER ⁶ JINYI YANG ⁷ EDUARDO BAÑADOS ⁸ MANUELA BISCHETTI ⁹
CHRISTOPHER CAIN ¹⁰ XIAOHUI FAN ¹ YOSHINOBU FUDAMOTO ^{11,1} SEYEDAZIM HASHEMI ⁶ RYOTA IKEDA ^{12,13}
ZHIYUAN JI ¹ XIANGYU JIN ¹ WEIZHE LIU ¹ YICHEN LIU ¹ JIANWEI LYU ¹ HAI-XIA MA ¹⁴
TSUTOMU T. TAKEUCHI ^{14,15} HIDEKI UMEHATA ^{16,17} FEIGE WANG ⁷ AND WEI LEONG TEE ¹

¹Steward Observatory, University of Arizona, 933 North Cherry Avenue, Tucson, AZ 85721, USA

²Kaoli Institute for Astronomy and Astrophysics, Peking University, Beijing 100871, China

³Department of Astronomy, School of Physics, Peking University, Beijing 100871, China

⁴Center for Astronomy and Astrophysics and Department of Physics, Fudan University, Shanghai 200438, China

⁵Department of Space, Earth, & Environment, Chalmers University of Technology, Chalmersplatsen 4 412 96 Gothenburg, Sweden

⁶Department of Physics & Astronomy, University of California, Riverside, CA 92521, USA

⁷Department of Astronomy, University of Michigan, 1085 S. University, Ann Arbor, MI 48109, USA

⁸Max-Planck-Institut für Astronomie, Königstuhl 17, D-69117 Heidelberg, Germany

⁹Dipartimento di Fisica, Sezione di Astronomia, Università di Trieste, via Tiepolo 11, 34143 Trieste, Italy

¹⁰School of Earth and Space Exploration, Arizona State University, Tempe, AZ 85287-6004, USA

¹¹Center for Frontier Science, Chiba University, 1-33 Yayoi-cho, Inage-ku, Chiba 263-8522, Japan

¹²Department of Astronomy, School of Science, SOKENDAI (The Graduate University for Advanced Studies), 2-21-1 Osawa, Mitaka, Tokyo 181-8588, Japan

¹³National Astronomical Observatory of Japan, 2-21-1 Osawa, Mitaka, Tokyo 181-8588, Japan

¹⁴Division of Particle and Astrophysical Science, Nagoya University, Furo-cho, Chikusa-ku, Nagoya 464-8602, Japan

¹⁵The Research Center for Statistical Machine Learning, the Institute of Statistical Mathematics, 10-3 Midori-cho, Tachikawa, Tokyo 190-8562, Japan

¹⁶Institute for Advanced Research, Nagoya University, Furocho, Chikusa, Nagoya 464-8602, Japan

¹⁷Department of Physics, Graduate School of Science, Nagoya University, Furocho, Chikusa, Nagoya 464-8602, Japan

Submitted to Nature Astronomy

ABSTRACT

Accreting supermassive black holes (SMBHs) regulate the evolution of their host galaxies through powerful outflows and multi-phase feedback (Kormendy & Ho 2013; Sun et al. 2025b). This process plays a crucial role in shaping SMBH-galaxy co-evolution across cosmic time (Inayoshi et al. 2020), but direct evidence linking nuclear winds to large-scale cold gas outflows, particularly in high-redshift quasars, has remained elusive. Here we present statistical evidence of a connection between nuclear winds and large-scale cold gas outflows in quasars at $z \sim 5.5$. Using stacked [C II] 158 μm emission profiles from ALMA observations, which trace galactic-scale neutral gas, we compare broad absorption line (BAL) quasars—tracing parsec- to sub-kiloparsec-scale nuclear winds (Weymann et al. 1991)—with non-BAL quasars. The BAL stack reveals a significant ($S/N=4.45$) broad component in the [C II] emission, indicating high-velocity neutral gas outflows with a velocity offset of $\Delta v_b = -2.1 \times 10^2 \text{ km s}^{-1}$ and a full width at half maximum of $1.18 \times 10^3 \text{ km s}^{-1}$, while the non-BAL stack shows no such feature. We estimate that a few percent up to one-quarter of the BAL wind energy is transferred to neutral gas on kiloparsec scales. These findings provide direct observational evidence that nuclear winds couple with galactic-scale neutral gas flows, supporting multi-phase AGN feedback models (Maiolino et al. 2012; Veilleux et al. 2020). This mechanism may contribute to explaining the diversity of M_{BH}/M_* ratios observed in some luminous AGN recently observed by JWST, compared to the Magorrian relation (e.g., Juodžbalis et al. 2024; Sun et al. 2025a).

1. INTRODUCTION

Quasars are powered by accretion onto supermassive black holes (SMBHs). Understanding whether and how quasars impact their host galaxies is crucial for investigating the co-evolution of SMBHs and galaxies (e.g., Kormendy & Ho 2013; Sun et al. 2025b), particularly in the early Universe. In this context, it is essential to

study how physics in the nuclear region influences the interstellar medium (ISM) on galactic scales.

The [C II] 158 μm fine-structure line is one of the strongest cooling lines of the ISM and serves as a key tracer of both star formation and gas dynamics (Stacey et al. 1991; Carilli & Walter 2013; Lagache et al. 2018). It provides insights into the properties of the cold ISM, typically at temperatures of $T \sim 10^2\text{--}10^3$ K, and has been extensively used in studies of galaxies across cosmic time (e.g., Gullberg et al. 2015; Jones et al. 2017). Broad wings in the [C II] line profile can indicate large-scale gas outflows driven by AGN or intense star formation (Cicone et al. 2015; Maiolino et al. 2012, see also Meyer et al. 2022; Salak et al. 2024). In addition, spatially extended [C II] morphologies provide complementary probes of large-scale disturbances such as mergers and companions (e.g., Neeleman et al. 2019; Bañados et al. 2019) and outflows (e.g., Bischetti et al. 2024; Carniani et al. 2018).

Previous studies have explored whether [C II] outflows correlate with various quasar properties, such as black hole mass, Eddington ratio, and redshift (e.g., Fiore et al. 2017; Venemans et al. 2020). These investigations found that AGN activity is often linked to broad [C II] emission features, suggesting that feedback processes may play a role in regulating star formation and galaxy growth (Harrison et al. 2018; Veilleux et al. 2020; Izumi et al. 2021a; Molina et al. 2023). However, despite these findings, there is limited direct observational evidence linking nuclear winds on parsec (or sub-kpc) scales with large-scale cold gas outflows.

An effective tracer of nuclear winds is the presence of broad absorption line (BAL) features in quasar spectra. BALs are associated with high-velocity outflows launched near the accretion disk and are observed in a significant fraction of luminous quasars (e.g., Weymann et al. 1991; Murray et al. 1995; Proga et al. 2000). These outflows can reach velocities of thousands of kilometers per second and are thought to originate from radiation-driven winds in the nuclear region (Elvis 2000). Bischetti et al. (2022) found that the fraction of BAL quasars is significantly higher during the epoch of reionization (XQR-30 program; D’Odorico et al. 2023). Investigating BAL-driven outflows at high redshift is particularly relevant for understanding SMBH-galaxy co-evolution, as early SMBHs observed so far exhibit a diversity in M_{BH}/M_* ratios relative to the local Magorrian relation (e.g., Sun et al. 2025a).

In this work, we investigate this connection using a sample of 17 quasars (16 used for stacking) at $z \sim 5.5$ —near the end of reionization (e.g., Bosman et al. 2022; Zhu et al. 2022). Our observations, conducted with ALMA and Keck/ESI, allow a consistent comparison between BAL and non-BAL quasars. By stacking the [C II] profiles, we have discovered an empirical link between nuclear winds and large-scale cold gas outflows in high-redshift quasars.

This paper is organized as follows. In Section 2, we describe the ALMA [C II] observations and Keck/ESI spectra of our quasar sample. Section 3 presents the main results of our [C II] profile analysis. In Section 4, we discuss the implications of our findings, and we summarize our conclusions in Section 5. Throughout this paper, we adopt the Planck18 cosmology (Planck Collaboration et al. 2020), implemented in `astropy` (Astropy Collaboration et al. 2018). All distances are quoted in proper units unless otherwise noted.

2. DATA

We select the brightest quasars in the z -band ($m_z \lesssim 20$) from Yang et al. (2017, 2019), identified through a systematic search for high-redshift quasars. These quasars fill the redshift gap near the end of reionization at $z \sim 5.5$, enabling us to investigate quasar properties in a previously underexplored epoch.

2.1. ALMA Observations

In Cycle 9 (2022.1.00662.S; PI: Zhu), we conducted ALMA Band 7 observations targeting 21 quasars at $z \sim 5.5$ from Yang et al. (2017, 2019), aiming to determine precise systemic redshifts ($\Delta z \sim 10^{-4}$) through [C II] 158 μm emission (details in Zhu et al. 2023a). Each observation employed two overlapping spectral windows fully covering the [C II] line at the expected redshift, alongside two additional spectral windows for dust continuum measurements. The observations used the C43-(1, 2, and 3) configurations, achieving an angular resolution of $\sim 1''$ across the entire sample.

Data calibration and reduction were performed using the CASA pipeline (version 6.4.1.12; McMullin et al. 2007; CASA Team et al. 2022). We generated data cubes and imaged the [C II] emission following procedures outlined in Eilers et al. (2020). Continuum subtraction was conducted in the uv -domain using all line-free channels across the four spectral windows by fitting a first-order polynomial. Imaging was performed with `tclean`, using natural weighting to optimize sensitivity. The average RMS noise level across the dataset is ~ 0.25 mJy beam $^{-1}$ per 30 MHz bin.

Spectra were extracted from sources within a single beam size to minimize contamination from extended [C II] emission, which could introduce complex kinematics. To assess the impact of aperture size, we also tested extraction using the standard 2-beam aperture, resulting in a decrease of the broad wing detection S/N from 4.45 (Section 3) to 3.3 for the BAL quasar stack, likely due to inclusion of additional host galaxy kinematic components. For the non-BAL quasar stack, the broad wing significance decreased from $< 2\sigma$ to below 1.5σ , indicating no significant detection.

We include only quasars with successful [C II] detections. Three quasars — J0157+3001, J1420-1602,

Table 1. Quasar Sample Used in This Work

No.	Quasar	RA (J2000)	Dec (J2000)	$z_{[\text{CII}]}$	M_{1450}	BI_0 (km s^{-1})	ESI
(1)	(2)	(3)	(4)	(5)	(6)	(7)	(8)
1	J0012+3632	00:12:32.88	+36:32:16.10	5.485 ± 0.001	-27.2	5650.9	2021-10
2	J0056+2241 ^a	00:56:56.04	+22:41:12.16	5.5218 ± 0.0002	-26.8	0.0	2022-09
3	J0120+2147	01:20:53.92	+21:47:06.20	5.4305 ± 0.0001	-26.5	0.0	2023-09
4	J0231-0728	02:31:37.64	-07:28:54.44	5.4227 ± 0.0005	-26.6	0.0	2013-01
5	J0306+1853	03:06:42.51	+18:53:15.85	5.3808 ± 0.0001	-28.9	0.0	2021-10
6	J1006-0310 ^b	10:06:14.61	-03:10:30.49	5.5149 ± 0.0004	-27.0	0.0	-
7	J1016+2541	10:16:37.70	+25:41:31.98	5.6797 ± 0.0004	-27.7	471.8	2024-06
8	J1022+2252	10:22:10.04	+22:52:25.44	5.4787 ± 0.0005	-27.3	1501.9	2016-03
9	J1048+3339 ^c	10:48:36.72	+33:39:47.66	5.6219 ± 0.0002	-27.0	0.0	-
10	J1335-0328	13:35:56.23	-03:28:38.20	5.699 ± 0.004	-27.8	304.8	2024-05
11	J1500+2816	15:00:36.83	+28:16:03.03	5.5727 ± 0.0006	-27.6	0.0	2024-06
12	J1513+0854	15:13:39.64	+08:54:06.58	5.4805 ± 0.0003	-26.8	0.0	2021-05
13	J1614+0114 ^c	16:14:35.35	+01:14:44.79	5.7945 ± 0.0004	-26.9	0.0	-
14	J1650+1617	16:50:42.25	+16:17:21.50	5.5769 ± 0.0001	-27.2	477.7	2021-05
15	J2207-0416	22:07:10.12	-04:16:56.28	5.5297 ± 0.0003	-27.8	2447.0	2021-10
16	J2317+2244	23:17:38.25	+22:44:09.63	5.558 ± 0.0002	-27.4	4329.0	2022-09
17	J2325+2628	23:25:14.24	+26:28:47.61	5.7514 ± 0.0001	-27.0	2676.2	2021-10

NOTE—Columns: (1) Index; (2) quasar name; (3) and (4) quasar coordinates (J2000); (5) [C II] redshift; (6) absolute magnitude at rest-frame 1450 Å, based on quasar luminosities from Yang et al. (2017, 2019); Zhu et al. (2023a); (7) balnicity, where strong BAL quasars ($\text{BI}_0 > 1000 \text{ km s}^{-1}$; see text for details) are marked in bold; (8) date of the most recent Keck/ESI observation.

a: outflow signature shown in the [C II] image.

b: see Yang et al. (2017) for spectra.

c: see Yang et al. (2019) for spectra.

and J1527+0641 — are excluded because the [C II] line may fall outside the spectral coverage. Additionally, J1133+1603 is excluded due to its close companion exhibiting a [C II] bridge suggesting interaction and complex gas kinematics (Zhu et al. 2024). The final ALMA sample comprises 17 quasars. The resulting [C II] images and spectra are presented in Figure 1. We determined the systemic redshift for each quasar by fitting a Gaussian profile to the [C II] emission line.

2.2. ESI Spectra

We acquired the Keck/ESI spectra for most quasars in this sample, which we use to identify BAL features in the rest frame UV. We conducted ESI observations for 13 quasars between 2021 and 2024 and retrieved archival spectra for one additional quasar. For the remaining three (J1006, J1048, and J1614), we used existing confirmation spectra from Yang et al. (2017, 2019), obtained with SSO-2.3m/WiFeS (Dopita et al. 2007, 2010) and Palomar-200-inch (P200)/DBSP.

The data were reduced using a custom IDL/GDL¹ pipeline, following procedures described in Becker et al. (2019) and Zhu et al. (2023a). This pipeline incorporates optimal sky subtraction techniques (Kelson 2003), one-dimensional spectral extraction (Horne 1986), and telluric absorption corrections based on the Cerro Paranal Advanced Sky Model (Noll et al. 2012; Jones et al. 2013). The extracted spectra have a pixel size of 15 km s^{-1} , with a typical velocity resolution of approximately 45 km s^{-1} (FWHM). The signal-to-noise ratio (S/N) per 30 km s^{-1} bin is greater than 10 near 1285 Å in the rest frame.

In this work, we focus on quasars with BAL outflows, i.e., classic BAL quasars, defined by a balnicity index $\text{BI}_0 > 0 \text{ km s}^{-1}$ (e.g., Weymann et al. 1991; Gibson et al. 2009). The balnicity index is computed using the equation:

¹ GNU Data Language (Coulais et al. 2010).

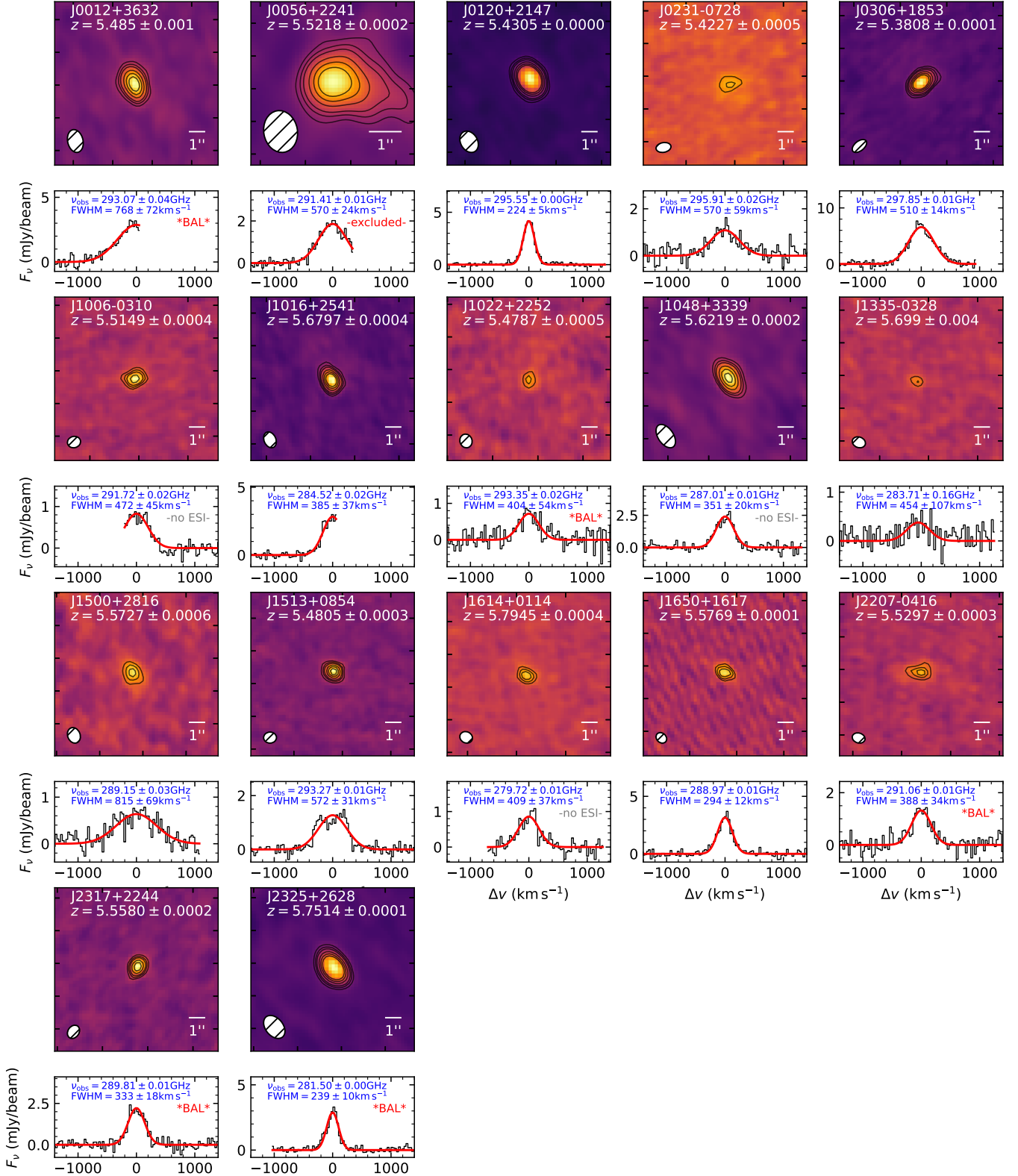


Figure 1. [C II] $158\mu\text{m}$ emission maps and spectra of the quasar sample observed with ALMA. Contours show (2σ , 3σ , 4σ , 6σ , 8σ , 10σ) levels. The synthesized beam is shown in the lower-left corner of each map. Measured redshifts are labeled for each quasar and red curves show the best Gaussian fits. Observed frequency and FWHM of the [C II] emission are also provided for reference. Quasars with significant BAL features are labeled, while those without ESI spectra are marked as “no ESI”. Since J0056 exhibits very extended [C II] emission in the image, it has been excluded from the stacking analysis.

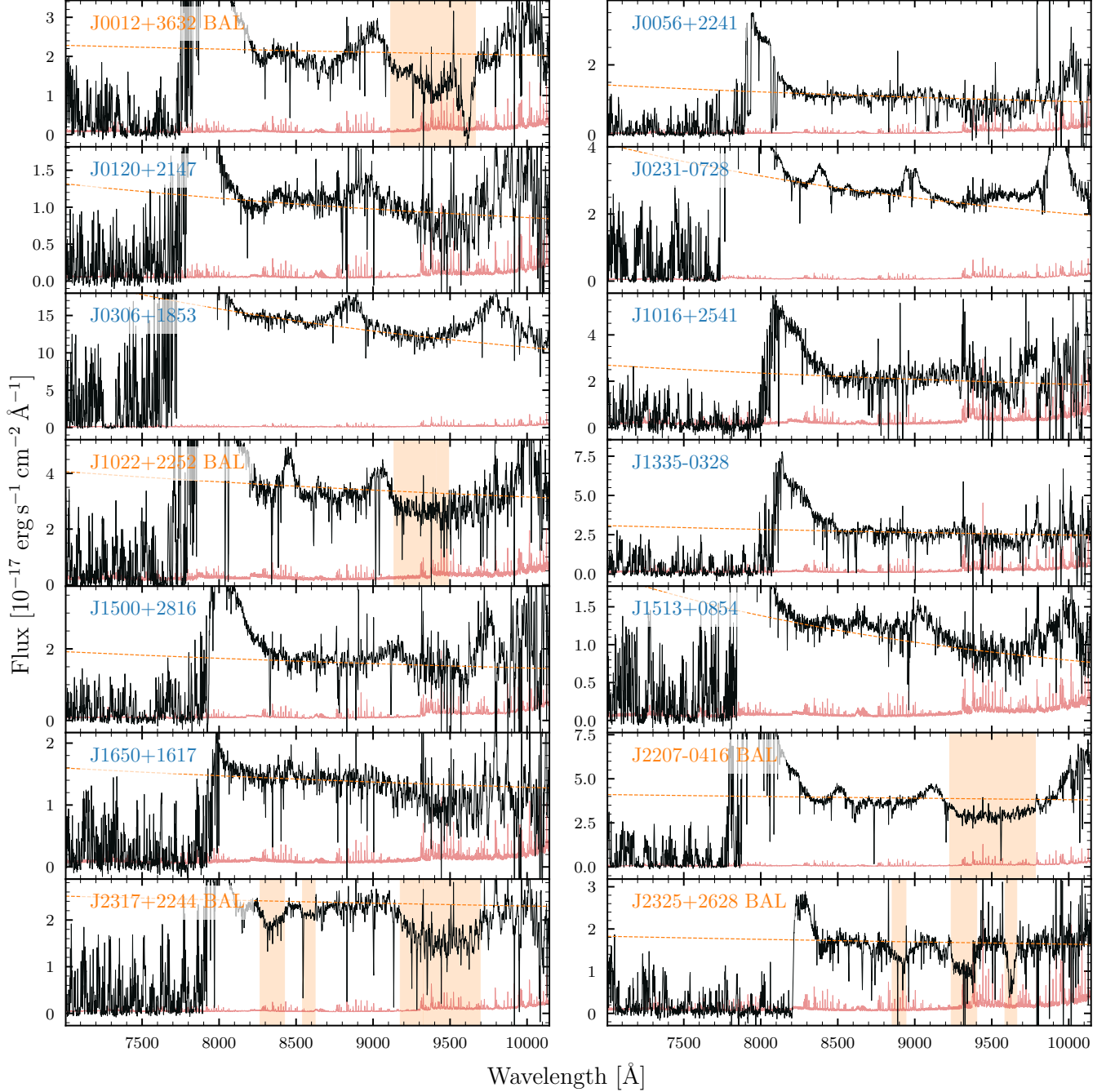


Figure 2. Keck/ESI rest-frame UV spectra of the quasar sample. Black and red colors plot the flux and corresponding error array, respectively. BAL quasars ($BI_0 > 1000 \text{ km s}^{-1}$) are labeled with orange text, and regions shaded in orange highlight prominent BAL absorption troughs. The dashed curves indicate the power-law continuum fits used to normalize the spectra.

$$BI_0 = \int_{v_{\min}}^{v_{\max}} \left(1 - \frac{f(v)}{0.9}\right) C(v) dv, \quad (1)$$

where $f(v)$ is the normalized flux as a function of velocity, $C(v)$ is a continuity function equal to 1 when absorption depth exceeds 10% over at least 2000 km s^{-1} , and 0 otherwise. We adopt $v_{\min} = 0 \text{ km s}^{-1}$ and $v_{\max} = 64500 \text{ km s}^{-1}$ (Bischetti et al. 2022).

We set zero velocity at C IV and identify BALs in both Si IV and C IV. Due to incomplete wavelength coverage, we do not attempt precise BI_0 measurements. A major source of uncertainty in computing BI_0 is the power-law continuum fitting. Three quasars (J1006, J1048, J1650) yield $BI_0 > 0$, but their BAL features are not visually apparent and may be influenced by telluric absorption or noise near spectral edges. To ensure robust-

ness, we classify only quasars with significant BAL features ($BI_0 > 1000 \text{ km s}^{-1}$) as BAL quasars. We identify five quasars meeting this criterion. Among our sample, J0012, J2317, and J2325 exhibit the most unambiguous BAL features ($BI_0 > 2500 \text{ km s}^{-1}$). As a consistency check, stacking [C II] emission for these three quasars alone yields a significant ($> 3\sigma$) broad [C II] wing (Section 3).

To compute $f(v)$, we normalized observed fluxes by fitting a power-law continuum to each quasar spectrum in the rest-frame wavelength range of 1285–1450 Å, masking strong emission or absorption lines. Figure 2 displays all ESI spectra, continuum fits, and BAL identifications. The detailed properties of our quasar sample are summarized in Table 1.

3. STACKED [C II] SPECTRA

We create stacked [C II] spectra for the five strong BAL quasars and eleven non-BAL quasars, respectively. The quasar J0056+2241 is excluded from both stacks due to its independently identified strong and extended [C II] feature in the emission line map. To construct the stacks, we normalize each spectrum by its peak flux, shift the [C II] emission line to the systemic redshift, and compute the mean stack in velocity space (Δv — the velocity offset relative to the systemic redshift) using bins of 60 km s^{-1} . The spectra are weighted by their inverse variance, although we verified that not weighting by inverse variance does not change the results, given the relatively consistent rms level across the entire quasar sample. We perform 1,000 bootstrap resamplings (with replacement) of 5 spectra from the BAL sample and 11 spectra from the non-BAL sample, respectively, to estimate the variance in the stacked profiles.

For the stacked spectra, we find that a single Gaussian profile centered at $\Delta v = 0$ cannot adequately describe the signal, especially for the BAL stack. Therefore, we fit a two-component Gaussian model: a narrow component with velocity dispersion $\sigma < 500 \text{ km s}^{-1}$ and a broad component with $\sigma > 500 \text{ km s}^{-1}$. The narrow component’s line center is fixed at $\Delta v = 0$, while the broad component’s center is allowed to vary. We derive uncertainties in the fit parameters based on the stacked fluxes across the bootstrap realizations.

Figure 3 panels (a) and (b) present the stacked [C II] profiles for the BAL and non-BAL samples, respectively. In the BAL stack, a single narrow Gaussian cannot fully explain the observed profile due to the presence of a significant blueshifted broad component. The residual broad emission is detected with a mean signal-to-noise ratio of 4.45 within its FWHM (i.e., a 4.45σ detection ²

² However, the σ value quoted here represents the signal detection level rather than a strict statistical significance, as there remains a $\lesssim 2\%$ probability that a stack of five non-BAL quasars could yield a similar broad component detection (see Section 4 and Figure 5).

). The best-fit Gaussian for the broad component yields a line center at $\Delta v_b = -2.1^{+1.3}_{-0.7} \times 10^2 \text{ km s}^{-1}$ and a FWHM of $1.18^{+0.39}_{-0.35} \times 10^3 \text{ km s}^{-1}$. We revisit the individual spectra in Figure 1 and notice that some BAL quasars show a slight gradual decrease in the flux toward the bottom of their single Gaussian fit; however, these features are too noisy to make robust measurements individually (e.g., J0012 and J2325). Nevertheless, these features become prominent in the stacked spectrum.

In contrast, the non-BAL stack does not exhibit a significant broad component, and the broad residual has a detection significance below 2σ . The Gaussian fit for the broad component is unconstrained. We note that the noise level in the non-BAL stack is lower than in the BAL stack due to the larger sample size. This reinforces the indication that the large-scale outflows traced by [C II] are predominantly associated with BAL quasars in our sample.

Additionally, we note that the narrow component of the BAL stack is narrower (FWHM = $3.2 \times 10^2 \text{ km s}^{-1}$) than that of the non-BAL case (FWHM = $4.3 \times 10^2 \text{ km s}^{-1}$). This difference might be attributed to viewing angle effects (see Section 4).

4. DISCUSSION

4.1. Potential Coupling of Nuclear Winds with the Cold ISM

The potential direct coupling between nuclear winds and the cold ISM may naturally explain the observed association between [C II] outflows and BAL outflows. Such coupling between multi-phase outflows is also seen in simulations (e.g., Tanner & Weaver 2022). We illustrate this process in the schematic diagram shown in Figure 3(c). If the BAL outflow is oriented toward the observer, we should observe blueshifted broad absorption in high-ionization lines, such as C IV and Si IV. These high-velocity nuclear winds may drive the outflow of gas on larger scales (\sim a few kpc) along the same direction, resulting in blueshifted broad [C II] emission. Conversely, when the viewing angle is different or the quasar is not sufficiently active to drive a BAL wind, we may not observe the blueshifted [C II] feature. Additionally, the narrower width of the narrow [C II] component in the BAL stack (FWHM = $3.2 \times 10^2 \text{ km s}^{-1}$) compared to the non-BAL stack (FWHM = $4.3 \times 10^2 \text{ km s}^{-1}$) may indicate a more face-on ³ orientation for BAL quasars. The broader [C II] emission in non-BAL quasars likely includes more complex host-galaxy kinematics, possibly due to a relatively more edge-on viewing geometry.

While our results suggest a strong link between nuclear winds and large-scale cold gas outflows, we note that [C II] outflows do not always appear blueshifted.

³ Note that there is usually a misalignment between the orientations of the accretion disk and the galaxy disk.

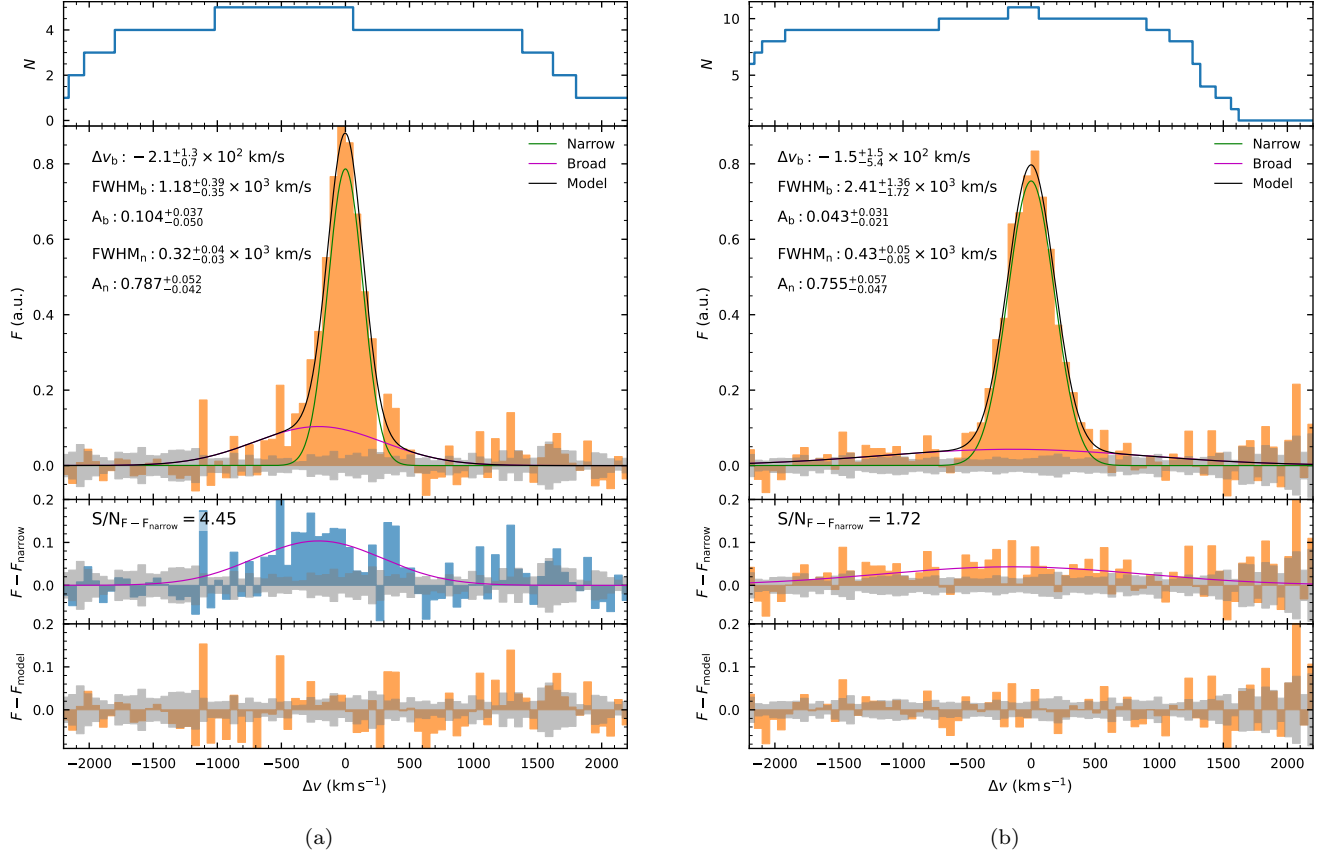


Figure 3. Stacked [C II] spectra and an illustration of quasar-driven outflows. **(a)** Stacked [C II] profile for the BAL quasar sample. The top panel shows the number of spectra contributing to the stack at each velocity bin (Δv). The middle panel displays the normalized [C II] flux, with the best-fit narrow (green) and broad (cyan) Gaussian components. The combined model is shown in black, with a broad component centered at $\Delta v_b = -2.1 \times 10^2$ km s⁻¹ and a FWHM of 1.18×10^3 km s⁻¹. The residuals between the total flux and the narrow component are shown in the third panel, highlighting the significance of the broad residual (mean $S/N = 4.45$). The bottom panel shows the overall residuals after subtracting the total model. **(b)** Stacked [C II] profile for the non-BAL quasar sample. The profile lacks a significant broad component, with residuals below 2σ . **(c)** A conceptual illustration of quasar outflows. The red region represents nuclear outflows traced by the BAL phase, while the diffuse blue region illustrates large-scale cold gas outflows traced by [C II]. This plot, not to physical scale, depicts the potential coupling between small-scale nuclear winds and galactic-scale outflows. The artwork was created by Y. Zhu using Adobe Fresco.

Redshifted outflows have also been observed (e.g., [Bischetti et al. 2019](#)), though such studies do not specifically distinguish between BAL and non-BAL quasars. These cases may correspond to scenarios where outflows are more complex, potentially involving interactions with the host galaxy or anisotropic ejection mechanisms. Understanding the full range of [C II] outflow orientations and kinematics will require further spatially resolved observations.

If our proposed scenario holds, we can estimate the coupling efficiency between BAL outflows and [C II] outflows. For the BAL outflows, we assume a nominal hydrogen column density $N_{\text{H}} = 10^{20.1 \sim 22.6} \text{ cm}^{-2}$ (e.g., [Xu et al. 2019](#)), and an outflow radius of $\log_{10}(R_{\text{out}}/\text{pc}) = 0 \sim 2$ (e.g., [Liu et al. 2022](#); [Veilleux et al. 2022](#); [Bischetti et al. 2024](#)). The mass outflow rate is given by

$$\dot{M}_{\text{BAL}} = 4\pi R_{\text{out}} N_{\text{H}} \mu m_{\text{p}} f_{\text{cov}} v_{\text{BAL}}, \quad (2)$$

where $v_{\text{BAL}} = 2.5 \times 10^4 \text{ km s}^{-1}$ is the mean velocity offset of the broad absorption troughs, $\mu = 1.4$ accounts for helium, and $f_{\text{cov}} = 0.2$ ([Hewett & Foltz 2003](#)) is the covering fraction. The kinetic power of the BAL outflow is

$$\dot{E}_{\text{BAL}} = \frac{1}{2} \dot{M}_{\text{BAL}} v_{\text{BAL}}^2 \approx 10^{44.3-46.3} \text{ erg s}^{-1}. \quad (3)$$

For the [C II] outflow, we adopt an outflow radius of 3.0 kpc, matching the mean ALMA beam size and consistent with the measurements in [Bischetti et al. \(2019\)](#). The fraction of the flux in the broad component over the total stacked flux is $F_{\text{broad}}/F_{\text{total}} = 0.32 \pm 0.11$. The outflow velocity is computed in the standard way following e.g., [Bischetti et al. \(2019\)](#):

$$v_{[\text{CII}]} = |\Delta v_{\text{b}}| + \frac{\text{FWHM}_{\text{broad}}}{2} = (8.0 \pm 2.1) \times 10^2 \text{ km s}^{-1}. \quad (4)$$

Following [Hailey-Dunsheath et al. \(2010\)](#), the outflow mass is given by

$$M_{\text{out}}/M_{\odot} = 0.77 \left(\frac{0.7 L_{[\text{CII}]}}{L_{\odot}} \right) \left(\frac{1.4 \times 10^{-4}}{X_{\text{C}^+}} \right) \times \frac{1 + 2e^{-91K/T} + n_{\text{crit}}/n}{2e^{-91K/T}}, \quad (5)$$

where $L_{[\text{CII}]}$ is the [C II] luminosity of the broad component determined by $F_{\text{broad}}/F_{\text{total}}$, $n_{\text{crit}} \sim 3 \times 10^3 \text{ cm}^{-3}$ is the critical density, and $X_{\text{C}^+} = 10^{-4}$ is the assumed abundance of C^+ (e.g., [Maiolino et al. 2012](#); [Bischetti et al. 2019](#)). Assuming $n \gg n_{\text{crit}}$ and a temperature range of $T \sim 100\text{--}1000 \text{ K}$, we obtain a mean outflow mass of $M_{\text{out}} = (9.3 \pm 0.2) \times 10^8 M_{\odot}$.

The time-averaged mass outflow rate is then given by

$$\dot{M}_{\text{out}} = \frac{v_{[\text{CII}]} \times M_{\text{out}}}{R_{\text{out}}} \approx 10^{2.3-2.4} M_{\odot} \text{ yr}^{-1}, \quad (6)$$

and the kinetic power by

$$\dot{E}_{\text{out}} = \frac{1}{2} \dot{M}_{\text{out}} \times v_{[\text{CII}]}^2 \approx 10^{43.6-43.8} \text{ erg s}^{-1}. \quad (7)$$

Finally, the coupling efficiency between the BAL and [C II] outflows is

$$\eta = \frac{\dot{E}_{\text{out}}}{\dot{E}_{\text{BAL}}} = 0.025_{-0.022}^{+0.23}. \quad (8)$$

This coupling efficiency suggests that BAL outflows may significantly contribute to neutral gas outflows, with a few percent to nearly one-quarter of the BAL energy injected into large-scale galactic outflows. However, this estimate relies on simplified assumptions, while BAL wind properties (e.g., N_{H} , outflow radius, and covering fraction) vary widely in the literature (e.g., [Veilleux et al. 2020](#); [Fiore et al. 2017](#)). Furthermore, BAL winds originate in the nuclear region, whereas [C II] outflows extend on kiloparsec scales, meaning their direct comparison is nontrivial. The energy coupled to neutral [C II] outflows represents only a fraction of the total energy injected by nuclear winds, implying that our coupling efficiency estimate may be a lower limit. Additionally, the observed [C II] outflows may trace the accumulated effect of past BAL-driven feedback rather than an ongoing nuclear wind phase.

For a conservative estimate, the cold gas mass outflow rate is $\sim 10^2 M_{\odot}/\text{yr}$. If these quasar hosts were Milky Way-mass galaxies (though unlikely), the escape velocity near the central 1 kpc would be $\sim 700 \text{ km s}^{-1}$ (e.g., [McMillan 2017](#); [Zhu et al. 2023b](#)). Since our measured outflow velocity is $\sim 800 \text{ km s}^{-1}$, the expelled gas should be capable of escaping the host galaxy. Given a typical quasar with $\log(L_{[\text{CII}]} / L_{\odot}) \sim 9$, corresponding to $\log(\text{SFR}) \sim 2$ (e.g., [Lagache et al. 2018](#)), our estimated outflow rate is comparable to the star formation rate. If a significant fraction of this outflowing gas is permanently removed from the galaxy or remains unavailable for star formation on short timescales, this could deplete the cold gas reservoir and suppress future star formation. However, additional constraints on gas recycling, inflows, and quasar duty cycles are needed to fully assess the long-term impact of these outflows on host galaxy evolution.

Considering the high BAL fraction in reionization-epoch bright quasars ($\sim 50\%$; [Bischetti et al. 2022](#)) and the link between BALs and [C II] outflows demonstrated here, this mechanism could influence the co-evolution of SMBHs and their host galaxies by modulating cold gas availability. While some quasars at high redshift exhibit M_{BH}/M_{*} ratios above the local Magorrian relation, such

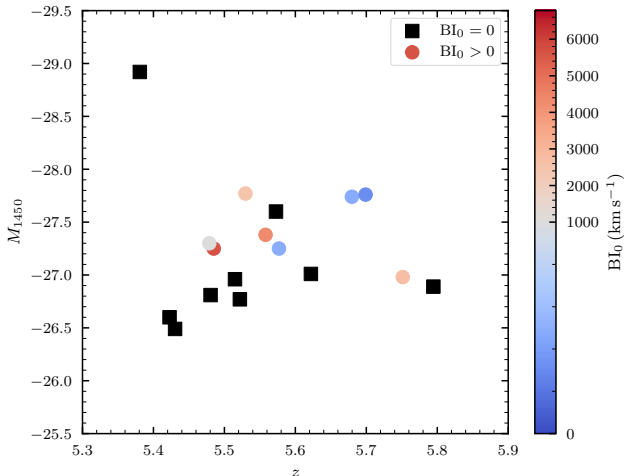


Figure 4. UV magnitude (M_{1450}) versus redshift for the quasars used in this work. The five quasars with strong BAL features ($BI_0 > 1000 \text{ km s}^{-1}$) are used to create the stacked [C II] profile shown in Figure 3(a).

deviations can be explained within the broader evolutionary context of black hole and galaxy growth, as well as observational biases, rather than requiring a systematic “overmassive” SMBH population (Sun et al. 2025a). The exact role of BAL-driven feedback remains uncertain, as some studies report enhanced star formation in quasar hosts (e.g., Molina et al. 2023), suggesting a more complex interplay between quasar activity, star formation, and gas dynamics.

4.2. Caveats and Potential Systematics

4.2.1. Intrinsic Properties of Quasars and Sample Size

Here, we discuss potential systematics and caveats that could influence our results. Previous studies have found a positive correlation between the incidence of [C II] outflows and quasar bolometric luminosity, suggesting that more luminous quasars are more likely to drive large-scale outflows (e.g., Bischetti et al. 2019; Maiolino et al. 2012). Since direct measurements of bolometric luminosity are not available for our sample, we use M_{1450} as a proxy, assuming a typical bolometric correction for high-redshift quasars. Figure 4 shows the distribution of our quasar sample in the M_{1450} versus redshift plane. Our sample spans a narrow redshift range, and both BAL and non-BAL quasars exhibit similar distributions in M_{1450} . This similarity reduces the likelihood that luminosity-related biases are responsible for the observed differences in [C II] profiles between the two samples.

To test whether the observed broad [C II] wing is driven by brighter quasars that preferentially exhibit BAL features, we divide the sample into two subgroups based on M_{1450} : quasars brighter than $M_{1450} = -27$ and those fainter than $M_{1450} = -27$. We stack the

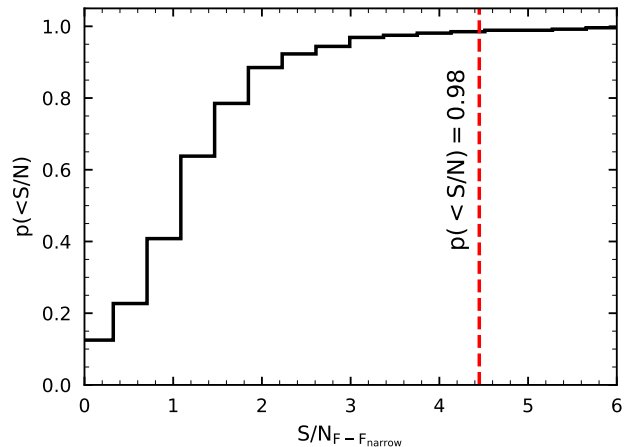


Figure 5. Cumulative distribution of the S/N of the broad component based on random stacks of five non-BAL quasars. The probability of reproducing an $S/N=4.4$ detection of the broad [C II] component in non-BAL quasars is less than 0.02. This test indicates that the observed broad component in the BAL quasar stack is unlikely to result from statistical fluctuations due to small sample size. Additionally, it suggests that systematic effects in data reduction or continuum subtraction are not responsible for the detection.

[C II] spectra separately for each subgroup and find no significant ($> 2\sigma$) detection of a broad residual or a systematically blueshifted [C II] line in either stack. This result suggests that quasar brightness is unlikely to be the primary factor driving the broad [C II] outflows in BAL quasars, at least within our sample.

Due to the absence of spectral coverage for Mg II or rest-frame optical emission lines, we cannot reliably constrain black hole masses or Eddington ratios for our sample. However, previous studies have shown that the occurrence of BAL features is not strongly correlated with these properties (e.g., Bischetti et al. 2023), mitigating potential concerns about their influence on our findings.

A significant remaining caveat is the lack of precise constraints on the host galaxy masses, as differences in host properties could affect the interpretation of our results. We note that the mean Gaussian FWHMs of individual quasars are similar between the BAL ($4.3 \times 10^2 \text{ km s}^{-1}$) and non-BAL ($4.6 \times 10^2 \text{ km s}^{-1}$) samples, suggesting no strong difference in dynamical masses. Additionally, without Mg II coverage, we cannot determine whether any BAL quasars in our sample belong to the low-ionization BAL (LoBAL) subclass, which might be intrinsically distinct (e.g., Bischetti et al. 2024). Therefore, we cannot determine if there are intrinsic physical differences between BAL and non-BAL host galaxies in our sample.

Nevertheless, we conduct an additional robustness check to verify that our detection of a broad [C II] component in the BAL quasar stack is not simply due to

statistical fluctuations arising from the small sample size or potential systematics from data reduction. We randomly select five quasars from the non-BAL group, stack their spectra, and measure the significance of any broad [C II] wing. Repeating this process multiple times (1,000 random trials), we find that the cumulative probability of randomly obtaining a broad wing with a significance equal to or greater than $S/N=4.4$ is less than 2% (Figure 5). This test strongly suggests that the broad [C II] component identified in the BAL quasar stack is unlikely to be a product of random noise fluctuations or systematic errors in data reduction, continuum subtraction, or spectral stacking. Consequently, the robust linkage we observe between nuclear BAL outflows and large-scale [C II] outflows is likely genuine.

4.2.2. Stacking Methods and Sample Selection

We note that Novak et al. (2020) reported no clear evidence of [C II] outflows in quasar host galaxies at $z > 6$, although their high-resolution observations were not optimized for detecting outflows on kiloparsec scales (see also Decarli et al. 2018; Sawamura et al. 2025). In their analysis, Novak et al. (2020) employed UV-plane stacking (in addition to the image-plane stacking) to enhance sensitivity and control for systematics arising from variable observing times and array configurations. In contrast, our dataset was collected using a uniform observational setup and consistent ALMA configurations, which already minimize these systematic concerns. Therefore, UV-plane stacking was unnecessary for our study. Nevertheless, as a consistency check, we performed image-plane stacking as shown in Figure A2, confirming that our main conclusions remain unaffected by this stacking method.

We caution that the method of continuum subtraction might still influence the visibility of the broad [C II] wing. However, we verified that using a zeroth-order polynomial continuum subtraction solely in the emission line spectral window in the uv domain does not change our results. Additionally, based on random stacking tests of non-BAL quasars (Figure 5), our continuum subtraction method is unlikely to introduce the observed blueshifted broad wing systematically. Throughout data reduction, we had no prior expectation of the broad [C II] component and consistently followed standard reduction procedures across the sample, further reducing potential systematic biases.

To examine the influence of individual quasars on our results, we conducted multiple tests:

1. The quasar J1513 exhibits a double-peaked [C II] profile, indicative of a rotating disk. Excluding this quasar does not affect our conclusions regarding the non-detection of a blueshifted broad component in the non-BAL stack.
2. Some ALMA spectra exhibit incomplete spectral coverage of the [C II] line (BAL: J0012; non-

BAL: J1006 and J1016). Excluding these quasars, we find the broad component remains significant, with a reduced S/N of 2.85 for the BAL group (expected due to the smaller sample size; otherwise, still $S/N > 3$ with 5 quasars) and 1.78 for the non-BAL group. Although J0012’s incomplete spectral coverage on the redshifted side may contribute to the detection of the broad wing, we argue that its intrinsic line profile — specifically, the presence of an extended wing — is the dominant factor in this contribution. As shown in Figure 1, J0012 exhibits a naturally broad [C II] profile, suggesting that the extended emission in the velocity space rather than spectral truncation is primarily responsible for its influence on the stacked spectrum.

3. To investigate the potential impact of host galaxy kinematics, we separated quasars into high- and low-FWHM groups (divided at 450 km s^{-1}). Neither group individually yields $> 3\sigma$ detection of a broad component (low-FWHM: 2.61σ , high-FWHM: 2.17σ), indicating that host galaxy kinematics alone do not explain the observed differences.
4. We tested normalization of spectra by their FWHM and amplitude. This normalization reduces the broad-component significance in the BAL group to 2.8σ , while the non-BAL group shows no significant broad component (1.0σ). However, this normalization might dilute weak broad wings, especially if the wing and the line core have different physical origins.
5. Excluding each BAL quasar individually (J0012, J1022, J2207, J2317, J2325) results in broad-component significances consistently greater than 2.8σ . The lowest significance (2.85σ) occurs when excluding J0012, which indeed individually exhibits an extended [C II] wing (Figure 1; and test No. 2) but only covers half of the spectral profile. Thus, our results do not critically depend on a single object.
6. For ESI spectra, due to limited wavelength coverage and uncertainties from telluric absorption, weak BAL features might be ambiguous. To address this, we separately stacked only the most robust BAL quasars ($BI_0 > 2500 \text{ km s}^{-1}$; J2317, J2325) against definitive non-BAL quasars ($BI_0 = 0$; J0120, J0231, J0306, J1500, J1513, J1614), normalizing by both amplitude and FWHM. We still detect a broad component at 2.38σ for the robust BAL subgroup versus 1.15σ for definitive non-BAL quasars, reinforcing the robustness of our conclusion despite smaller samples.

In future works, performing stacking analyses with larger samples and more comprehensive spectral coverage would help verify and expand upon these conclusions.

4.3. Individual Quasar: J0056+2241

Among our quasar sample, the non-BAL quasar J0056+2241 exhibits an exceptionally extended morphology in its [C II] emission map, with a tail extending over $2''.5$ (corresponding to ~ 15 kpc) toward the southwest from the quasar center. The moment 1 map (Figure A1) reveals blueshifted emission within the extended [C II] structure, with a velocity offset of ~ -100 – 150 km s^{-1} , although this velocity remains within the width of its emission line profile (FWHM = 570 km s^{-1} ; Figure 1). This large-scale structure may indicate a significant outflow of cold gas on galactic scales, possibly driven by strong AGN activity. However, such an extended structure could also result from other processes, such as a merger (e.g., Bañados et al. 2019; Izumi et al. 2021b).

Interestingly, despite this potential morphological evidence of outflows, the ESI spectrum of J0056+2241 does not show strong BAL features. However, there is a notable flux discontinuity redward of the $\text{Ly}\alpha + [\text{N V}]$ emission complex. Additionally, the $\text{Ly}\alpha$ line itself is associated with strong absorption features, as also noted in Zhu et al. (2023a). These absorbers may indicate the presence of intervening gas clouds or infalling material along the line of sight.

One potential explanation for the lack of BAL features is that the outflows in J0056+2241 may not be well-aligned with our line of sight. Indeed, we do not see strong blueshifted [C II] emission, suggesting that the [C II] outflow is also not aligned along our line of sight. In this scenario, the outflow may be oriented at an angle where high-velocity winds do not produce strong absorption features in the rest-frame UV spectrum. Alternatively, the outflow may be dominated by dense, neutral gas phases that are less effective at producing BAL signatures in high-ionization species such as C IV and Si IV.

Another possibility is a difference in timescales between nuclear and galactic-scale outflows. If the large-scale outflow observed in [C II] is a remnant of past AGN activity, the current nuclear wind may no longer be strong enough to produce detectable BAL features in the UV. Alternatively, J0056+2241 may be in an early stage of outflow development, where neutral gas has already been accelerated to large scales, but the ionized phase has not yet fully developed. Further spatially resolved spectroscopic observations, particularly in ionized and molecular gas tracers, could help disentangle the structure and dynamics of the outflow in J0056+2241, providing additional insight into the feedback mechanisms in this system.

Finally, as a sanity check, including J0056+2241 in our non-BAL quasar stack increases the significance of the broad component only from 1.72σ to 1.77σ , which is slightly higher than when excluding J0056+2241. This suggests that its extended [C II] emission may contribute modestly to the overall broad wing detected in the stacked profile.

5. SUMMARY

We present evidence for a connection between nuclear winds and large-scale cold gas outflows in high-redshift ($z \sim 5.5$) quasars by comparing stacked [C II] emission profiles for BAL and non-BAL quasar samples. Our key findings are as follows:

1. The stacked [C II] spectrum for BAL quasars reveals a significant blueshifted broad component, indicating the presence of high-velocity outflows with a velocity offset of $\Delta v_b = -2.1 \times 10^2$ km s^{-1} and a FWHM of 1.18×10^3 km s^{-1} . In contrast, the non-BAL quasar stack shows no significant broad component.
2. We estimate a coupling efficiency of $\eta = 0.025_{-0.022}^{+0.23}$ between BAL-driven outflows and cold gas outflows traced by [C II]. This suggests that a few percent to up to one-quarter of the BAL outflow energy may be injected into neutral gas on galactic scales and contribute to multi-phase feedback processes.
3. An individual quasar, J0056+2241, exhibits an extended [C II] morphology spanning 15 kpc, despite lacking strong BAL features, potentially due to the outflow orientation relative to the line of sight. Alternatively, it may be a merging system.

These results highlight the multi-phase, multi-scale nature of AGN-driven feedback in high-redshift quasars. They suggest that nuclear winds may play a crucial role in regulating cold gas outflows and potentially influencing galaxy evolution in the early universe. Given the significantly higher fraction of BAL quasars observed during the epoch of reionization ($\sim 50\%$; Bischetti et al. 2022), our findings suggest that BAL-driven feedback may contribute to explaining the observed diversity in SMBH-to-host mass ratios at high redshifts (e.g., Sun et al. 2025a).

ACKNOWLEDGMENTS

YZ, MJR, YS, GHR, and ZJ acknowledge support from the NIRCAM Science Team contract to the University of Arizona, NAS5-02015. This work was supported by the NSF through award SOSPADA-029 from the NRAO. YZ and GDB were supported by the NSF through grant AST-1751404. LCH was supported by the National Science Foundation of China (12233001) and the National Key R&D Program of

China (2022YFF0503401). FY is supported by the Natural Science Foundation of China (grants 12133008, 12192220, 12192223, and 12361161601), the China Manned Space Program through its Space Application System, and the National Key R&D Program of China No. 2023YFB3002502. TTT has been supported by the Japan Society for the Promotion of Science (JSPS) Grants-in-Aid for Scientific Research (24H00247). This work has also been supported in part by the Collaboration Funding of the Institute of Statistical Mathematics “Machine-Learning-Based Cosmogony: From Structure Formation to Galaxy Evolution”.

This paper makes use of the following ALMA data: ADS/JAO.ALMA#2022.1.00662.S. ALMA is a partnership of ESO (representing its member states), NSF (USA) and NINS (Japan), together with NRC (Canada), MOST and ASIAA (Taiwan), and KASI (Republic of Korea), in cooperation with the Republic of Chile. The Joint ALMA Observatory is operated by ESO, AUI/NRAO and NAOJ. The National Radio Astronomy Observatory and Green Bank Observatory are facilities of the U.S. National Science Foundation operated under cooperative agreement by Associated Universities, Inc.

Some of the data presented herein were obtained at Keck Observatory, which is a private 501(c)3 non-profit

organization operated as a scientific partnership among the California Institute of Technology, the University of California, and the National Aeronautics and Space Administration. The Observatory was made possible by the generous financial support of the W. M. Keck Foundation. The authors wish to recognize and acknowledge the very significant cultural role and reverence that the summit of Maunakea has always had within the Native Hawaiian community. We are most fortunate to have the opportunity to conduct observations from this mountain.

This manuscript benefited from grammar checking and proofreading using ChatGPT (OpenAI; <https://openai.com/chatgpt>).

Author Contributions: YZ led the observations and data reduction for the ALMA and ESI programs, performed the initial analysis, and wrote the first draft. MJR, LCH, YS, GHR, and FY contributed to the initial discussions and interpretation of the results. TJLCB, GDB, and JY assisted with observations and sample selection. EB and MB contributed to the analysis methodology and statistical interpretation. The remaining authors provided helpful comments and discussions.

APPENDIX

A. SUPPLEMENTARY FIGURES

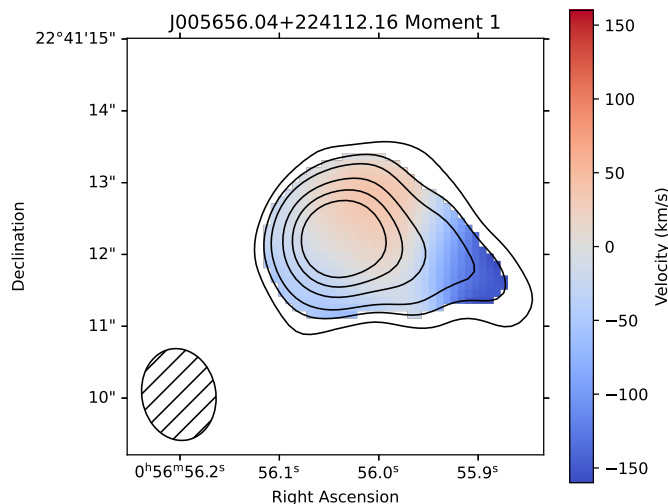


Figure A1. The moment 1 (velocity) map of J0056+2241 relative to its systemic redshift of $z = 5.5218$. The contours represent significance levels of $(2\sigma, 3\sigma, 4\sigma, 6\sigma, 8\sigma, 10\sigma)$ from the moment 0 map. The map reveals blueshifted emission within the extended [CII] structure, although the velocity remains within the FWHM of its emission line profile, as shown in Figure 1.

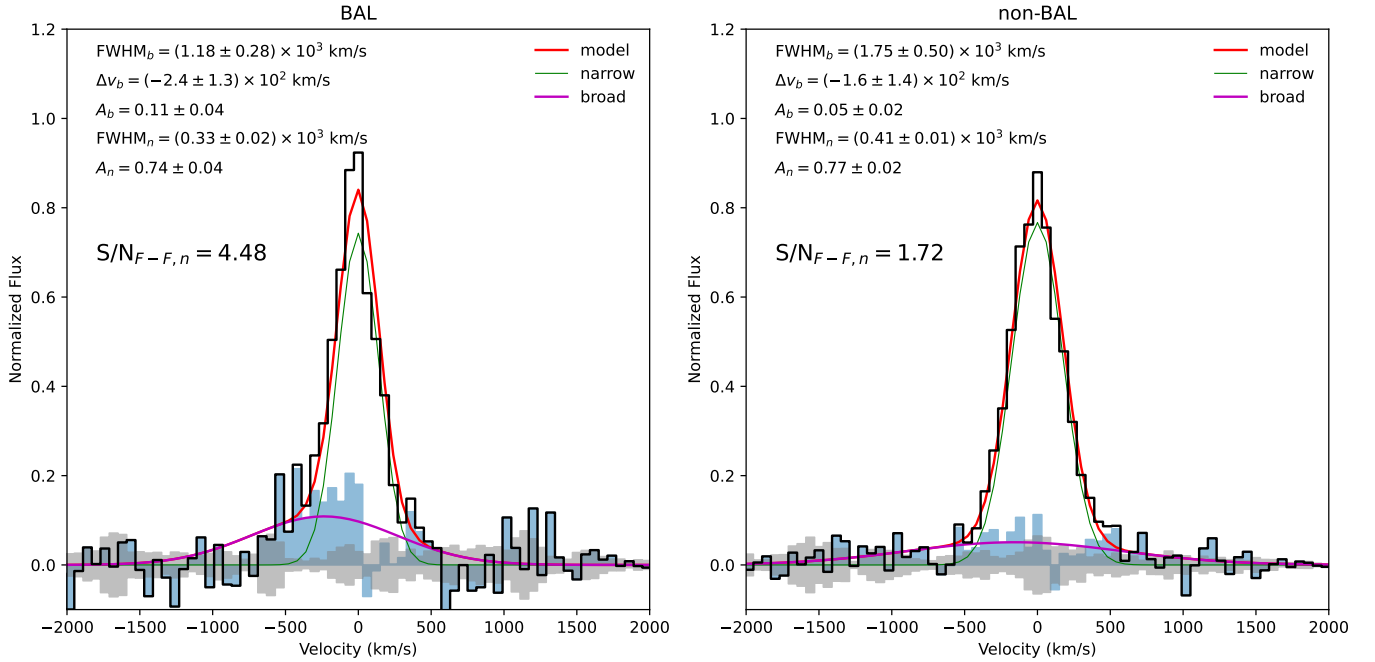


Figure A2. [C II] emission from the stacked image cubes of BAL (left panel) and non-BAL (right panel) quasars. The black curves represent the normalized flux (arbitrary units), while the blue shaded regions show the residual flux after subtracting the narrow component. The gray shaded regions indicate the $\pm 1\sigma$ noise level. The fitting parameter uncertainties shown in this plot are derived from a single stack, rather than the bootstrap approach used in Figure 3. When stacking image cubes instead of 1D spectra, the BAL sample still exhibits a significant broad component at 4.48σ , whereas the non-BAL sample remains below the 2σ detection threshold.

REFERENCES

- Astropy Collaboration, Price-Whelan, A. M., Sip{\H{o}}cz, B. M., et al. 2018, *AJ*, 156, 123, doi: [10.3847/1538-3881/aab4f](https://doi.org/10.3847/1538-3881/aab4f)
- Bañados, E., Novak, M., Neeleman, M., et al. 2019, *ApJ*, 881, L23, doi: [10.3847/2041-8213/ab3659](https://doi.org/10.3847/2041-8213/ab3659)
- Becker, G. D., Pettini, M., Rafelski, M., et al. 2019, *ApJ*, 883, 163, doi: [10.3847/1538-4357/ab3eb5](https://doi.org/10.3847/1538-4357/ab3eb5)
- Bischetti, M., Maiolino, R., Carniani, S., et al. 2019, *A&A*, 630, A59, doi: [10.1051/0004-6361/201833557](https://doi.org/10.1051/0004-6361/201833557)
- Bischetti, M., Feruglio, C., D’Odorico, V., et al. 2022, *Nature*, 605, 244, doi: [10.1038/s41586-022-04608-1](https://doi.org/10.1038/s41586-022-04608-1)
- Bischetti, M., Fiore, F., Feruglio, C., et al. 2023, The fraction and kinematics of broad absorption line quasars across cosmic time, doi: [10.48550/arXiv.2301.09731](https://doi.org/10.48550/arXiv.2301.09731)
- Bischetti, M., Choi, H., Fiore, F., et al. 2024, *ApJ*, 970, 9, doi: [10.3847/1538-4357/ad4a77](https://doi.org/10.3847/1538-4357/ad4a77)
- Bosman, S. E. I., Davies, F. B., Becker, G. D., et al. 2022, *MNRAS*, 514, 55, doi: [10.1093/mnras/stac1046](https://doi.org/10.1093/mnras/stac1046)
- Carilli, C. L., & Walter, F. 2013, *ARA&A*, 51, 105, doi: [10.1146/annurev-astro-082812-140953](https://doi.org/10.1146/annurev-astro-082812-140953)
- Carniani, S., Maiolino, R., Smit, R., & Amorín, R. 2018, *ApJ*, 854, L7, doi: [10.3847/2041-8213/aaab45](https://doi.org/10.3847/2041-8213/aaab45)
- CASA Team, Bean, B., Bhatnagar, S., et al. 2022, *PASP*, 134, 114501, doi: [10.1088/1538-3873/ac9642](https://doi.org/10.1088/1538-3873/ac9642)
- Cicone, C., Maiolino, R., Gallerani, S., et al. 2015, *A&A*, 574, A14, doi: [10.1051/0004-6361/201424980](https://doi.org/10.1051/0004-6361/201424980)
- Coulaï, A., Schellens, M., Gales, J., et al. 2010, 434, 187, doi: [10.48550/arXiv.1101.0679](https://doi.org/10.48550/arXiv.1101.0679)
- Decarli, R., Walter, F., Venemans, B. P., et al. 2018, *ApJ*, 854, 97, doi: [10.3847/1538-4357/aaa5aa](https://doi.org/10.3847/1538-4357/aaa5aa)
- D’Odorico, V., Bañados, E., Becker, G. D., et al. 2023, *MNRAS*, 523, 1399, doi: [10.1093/mnras/stad1468](https://doi.org/10.1093/mnras/stad1468)
- Dopita, M., Hart, J., McGregor, P., et al. 2007, *Astrophysics and Space Science*, 310, 255, doi: [10.1007/s10509-007-9510-z](https://doi.org/10.1007/s10509-007-9510-z)
- Dopita, M., Rhee, J., Farage, C., et al. 2010, *Astrophysics and Space Science*, 327, 245, doi: [10.1007/s10509-010-0335-9](https://doi.org/10.1007/s10509-010-0335-9)
- Eilers, A.-C., Hennawi, J. F., Decarli, R., et al. 2020, *ApJ*, 900, 37, doi: [10.3847/1538-4357/aba52e](https://doi.org/10.3847/1538-4357/aba52e)
- Elvis, M. 2000, *ApJ*, 545, 63, doi: [10.1086/317778](https://doi.org/10.1086/317778)
- Fiore, F., Feruglio, C., Shankar, F., et al. 2017, *A&A*, 601, A143, doi: [10.1051/0004-6361/201629478](https://doi.org/10.1051/0004-6361/201629478)

- Gibson, R. R., Jiang, L., Brandt, W. N., et al. 2009, *ApJ*, 692, 758, doi: [10.1088/0004-637X/692/1/758](https://doi.org/10.1088/0004-637X/692/1/758)
- Gullberg, B., De Breuck, C., Vieira, J. D., et al. 2015, *MNRAS*, 449, 2883, doi: [10.1093/mnras/stv372](https://doi.org/10.1093/mnras/stv372)
- Hailey-Dunsheath, S., Nikola, T., Stacey, G. J., et al. 2010, *ApJ*, 714, L162, doi: [10.1088/2041-8205/714/1/L162](https://doi.org/10.1088/2041-8205/714/1/L162)
- Harrison, C. M., Costa, T., Tadhunter, C. N., et al. 2018, *Nature Astronomy*, 2, 198, doi: [10.1038/s41550-018-0403-6](https://doi.org/10.1038/s41550-018-0403-6)
- Hewett, P. C., & Foltz, C. B. 2003, *AJ*, 125, 1784, doi: [10.1086/368392](https://doi.org/10.1086/368392)
- Horne, K. 1986, *PASP*, 98, 609, doi: [10.1086/131801](https://doi.org/10.1086/131801)
- Inayoshi, K., Visbal, E., & Haiman, Z. 2020, *ARA&A*, 58, 27, doi: [10.1146/annurev-astro-120419-014455](https://doi.org/10.1146/annurev-astro-120419-014455)
- Izumi, T., Onoue, M., Matsuoka, Y., et al. 2021a, *ApJ*, 908, 235, doi: [10.3847/1538-4357/abd7ef](https://doi.org/10.3847/1538-4357/abd7ef)
- Izumi, T., Matsuoka, Y., Fujimoto, S., et al. 2021b, *ApJ*, 914, 36, doi: [10.3847/1538-4357/abf6dc](https://doi.org/10.3847/1538-4357/abf6dc)
- Jones, A., Noll, S., Kausch, W., Szyszka, C., & Kimeswenger, S. 2013, *A&A*, 560, A91, doi: [10.1051/0004-6361/201322433](https://doi.org/10.1051/0004-6361/201322433)
- Jones, G. C., Carilli, C. L., Shao, Y., et al. 2017, *ApJ*, 850, 180, doi: [10.3847/1538-4357/aa8df2](https://doi.org/10.3847/1538-4357/aa8df2)
- Juodžbalis, I., Maiolino, R., Baker, W. M., et al. 2024, *Nature*, 636, 594, doi: [10.1038/s41586-024-08210-5](https://doi.org/10.1038/s41586-024-08210-5)
- Kelson, D. D. 2003, *PASP*, 115, 688, doi: [10.1086/375502](https://doi.org/10.1086/375502)
- Kormendy, J., & Ho, L. C. 2013, *ARA&A*, 51, 511, doi: [10.1146/annurev-astro-082708-101811](https://doi.org/10.1146/annurev-astro-082708-101811)
- Lagache, G., Cousin, M., & Chatzikos, M. 2018, *A&A*, 609, A130, doi: [10.1051/0004-6361/201732019](https://doi.org/10.1051/0004-6361/201732019)
- Liu, W., Veilleux, S., Rupke, D. S. N., et al. 2022, *ApJ*, 934, 160, doi: [10.3847/1538-4357/ac7a46](https://doi.org/10.3847/1538-4357/ac7a46)
- Maiolino, R., Gallerani, S., Neri, R., et al. 2012, *MNRAS*, 425, L66, doi: [10.1111/j.1745-3933.2012.01303.x](https://doi.org/10.1111/j.1745-3933.2012.01303.x)
- McMillan, P. J. 2017, *MNRAS*, 465, 76, doi: [10.1093/mnras/stw2759](https://doi.org/10.1093/mnras/stw2759)
- McMullin, J. P., Waters, B., Schiebel, D., Young, W., & Golap, K. 2007, 376, 127. <https://ui.adsabs.harvard.edu/abs/2007ASPC..376..127M>
- Meyer, R. A., Walter, F., Cicone, C., et al. 2022, *ApJ*, 927, 152, doi: [10.3847/1538-4357/ac4e94](https://doi.org/10.3847/1538-4357/ac4e94)
- Molina, J., Ho, L. C., Wang, R., et al. 2023, *ApJ*, 944, 30, doi: [10.3847/1538-4357/aca9b](https://doi.org/10.3847/1538-4357/aca9b)
- Murray, N., Chiang, J., Grossman, S. A., & Voit, G. M. 1995, *ApJ*, 451, 498, doi: [10.1086/176238](https://doi.org/10.1086/176238)
- Neeleman, M., Bañados, E., Walter, F., et al. 2019, *ApJ*, 882, 10, doi: [10.3847/1538-4357/ab2ed3](https://doi.org/10.3847/1538-4357/ab2ed3)
- Noll, S., Kausch, W., Barden, M., et al. 2012, *A&A*, 543, A92, doi: [10.1051/0004-6361/201219040](https://doi.org/10.1051/0004-6361/201219040)
- Novak, M., Venemans, B. P., Walter, F., et al. 2020, *ApJ*, 904, 131, doi: [10.3847/1538-4357/abc33f](https://doi.org/10.3847/1538-4357/abc33f)
- Planck Collaboration, Aghanim, N., Akrami, Y., et al. 2020, *A&A*, 641, A6, doi: [10.1051/0004-6361/201833910](https://doi.org/10.1051/0004-6361/201833910)
- Proga, D., Stone, J. M., & Kallman, T. R. 2000, *ApJ*, 543, 686, doi: [10.1086/317154](https://doi.org/10.1086/317154)
- Salak, D., Hashimoto, T., Inoue, A. K., et al. 2024, *ApJ*, 962, 1, doi: [10.3847/1538-4357/ad0df5](https://doi.org/10.3847/1538-4357/ad0df5)
- Sawamura, M., Izumi, T., Nakanishi, K., et al. 2025, *ApJ*, 980, 121, doi: [10.3847/1538-4357/ada943](https://doi.org/10.3847/1538-4357/ada943)
- Stacey, G. J., Geis, N., Genzel, R., et al. 1991, *ApJ*, 373, 423, doi: [10.1086/170062](https://doi.org/10.1086/170062)
- Sun, Y., Rieke, G. H., Lyu, J., et al. 2025a, The M_{*} - M_{BH} Relation Evolution from $z \sim 6$ to the Present Epoch, doi: [10.48550/arXiv.2503.03675](https://doi.org/10.48550/arXiv.2503.03675)
- Sun, Y., Lyu, J., Rieke, G. H., et al. 2025b, *ApJ*, 978, 98, doi: [10.3847/1538-4357/ad973b](https://doi.org/10.3847/1538-4357/ad973b)
- Tanner, R., & Weaver, K. A. 2022, *AJ*, 163, 134, doi: [10.3847/1538-3881/ac4d23](https://doi.org/10.3847/1538-3881/ac4d23)
- Veilleux, S., Maiolino, R., Bolatto, A. D., & Aalto, S. 2020, *Astronomy and Astrophysics Review*, 28, 2, doi: [10.1007/s00159-019-0121-9](https://doi.org/10.1007/s00159-019-0121-9)
- Veilleux, S., Rupke, D. S. N., Liu, W., et al. 2022, *ApJ*, 926, 60, doi: [10.3847/1538-4357/ac3cbb](https://doi.org/10.3847/1538-4357/ac3cbb)
- Venemans, B. P., Walter, F., Neeleman, M., et al. 2020, *ApJ*, 904, 130, doi: [10.3847/1538-4357/abc563](https://doi.org/10.3847/1538-4357/abc563)
- Weymann, R. J., Morris, S. L., Foltz, C. B., & Hewett, P. C. 1991, *ApJ*, 373, 23, doi: [10.1086/170020](https://doi.org/10.1086/170020)
- Xu, X., Arav, N., Miller, T., & Benn, C. 2019, *ApJ*, 876, 105, doi: [10.3847/1538-4357/ab164e](https://doi.org/10.3847/1538-4357/ab164e)
- Yang, J., Fan, X., Wu, X.-B., et al. 2017, *AJ*, 153, 184, doi: [10.3847/1538-3881/aa6577](https://doi.org/10.3847/1538-3881/aa6577)
- Yang, J., Wang, F., Fan, X., et al. 2019, *ApJ*, 871, 199, doi: [10.3847/1538-4357/aaf858](https://doi.org/10.3847/1538-4357/aaf858)
- Zhu, Y., Becker, G. D., Bosman, S. E. I., et al. 2022, *ApJ*, 932, 76, doi: [10.3847/1538-4357/ac6e60](https://doi.org/10.3847/1538-4357/ac6e60)
- Zhu, Y., Becker, G. D., Christenson, H. M., et al. 2023a, *ApJ*, 955, 115, doi: [10.3847/1538-4357/aceef4](https://doi.org/10.3847/1538-4357/aceef4)
- Zhu, Y., Ma, H.-X., Dong, X.-B., et al. 2023b, *MNRAS*, 519, 4479, doi: [10.1093/mnras/stac3483](https://doi.org/10.1093/mnras/stac3483)
- Zhu, Y., Bakx, T. J. L. C., Ikeda, R., et al. 2024, *RNAAS*, 8, 284, doi: [10.3847/2515-5172/ad91ad](https://doi.org/10.3847/2515-5172/ad91ad)